CODE-CL: COnceptor-Based Gradient Projection for DEep Continual Learning

Marco P. E. Apolinario   Kaushik Roy

Elmore Family School of Electrical and Computer Engineering

Purdue University, West Lafayete, IN 47906

mapolina@purdue.edu, kaushik@purdue.edu

Abstract

Continual learning, or the ability to progressively integrate new concepts, is fundamental to intelligent beings, enabling adaptability in dynamic environments. In contrast, artificial deep neural networks face the challenge of catastrophic forgetting when learning new tasks sequentially. To alleviate the problem of forgetting, recent approaches aim to preserve essential weight subspaces for previous tasks by limiting updates to orthogonal subspaces via gradient projection. While effective, this approach can lead to suboptimal performance, particularly when tasks are highly correlated. In this work, we introduce COnceptor-based gradient projection for DEep Continual Learning (CODE-CL), a novel method that leverages conceptor matrix representations, a computational model inspired by neuroscience, to more flexibly handle highly correlated tasks. CODE-CL encodes directional importance within the input space of past tasks, allowing new knowledge integration in directions modulated by $1 - S$, where S represents the direction's relevance for prior tasks. Additionally, we analyze task overlap using conceptor-based representations to identify highly correlated tasks, facilitating efficient forward knowledge transfer through scaled projection within their intersecting subspace. This strategy enhances flexibility, allowing learning in correlated tasks without significantly disrupting previous knowledge. Extensive experiments on continual learning image classification benchmarks validate CODE-CL's efficacy, showcasing superior performance with minimal forgetting, outperforming most state-of-the-art methods.

1. Introduction

The ability to continually acquire, retain, and adapt knowledge over time is a defining characteristic of intelligent behavior in humans and animals. This capacity to learn incrementally from new information, while retaining past knowledge, enables adaptation to dynamic and unpredictable environments [11, 14, 19]. In contrast, conventional deep learning models typically excel when trained in a static, batch-based manner on fixed datasets, but they face significant difficulties when adapting to new information sequentially without revisiting previous data, a limitation known as catastrophic forgetting [8, 14, 30]. This phenomenon, where knowledge of previous tasks degrades as new tasks are learned, poses a fundamental obstacle to achieving continual learning (CL) in artificial neural networks.

Recent research in continual learning has led to the development of strategies aimed at mitigating catastrophic forgetting while enabling the integration of new information. These strategies broadly fall into three categories: regularization-based, expansion-based, and memory-based methods. Regularization-based methods seek to constrain updates to important model parameters for previous tasks, preserving essential features while allowing flexibility in unimportant regions of the parameter space [12, 18, 27, 28, 36]. Expansion-based methods dynamically allocate new network resources to accommodate the growing complexity of sequential tasks [20, 23, 32–34]. Memory-based approaches, by contrast, store representative samples or features from previous tasks to maintain performance on earlier data distributions [2, 3, 6, 17, 21, 25, 31, 35]. While each of these approaches provides valuable contributions, they often require trade-offs between flexibility and retention, and many still rely on extensive memory storage or the allocation of dedicated resources for each new task.

A promising direction in the pursuit of efficient and scalable continual learning involves leveraging gradient projection methods, a group of techniques within the memory-based approaches. Recent work in this area [6, 7, 9, 16, 24, 25, 31, 35] aims to preserve essential subspaces in the weight vector space of neural networks that correspond to previously learned tasks. By restricting model updates to orthogonal subspaces, through projecting gradients into those subspaces, these methods effectively limit interference with prior knowledge, thereby reducing catastrophic forgetting. However, subspace-restricting gradients face inherent limitations, as they often exclude potentially beneficial regions of the weight space, thereby limiting the model's capac-

ity to fully utilize shared information across tasks. This restriction is particularly problematic in scenarios where tasks share common characteristics, as such overlap could be leveraged for positive forward transfer of knowledge [4, 16, 24].

In this work, we propose COnceptor-based gradient projection for DEep Continual Learning (CODE-CL), a novel method that extends gradient projection approaches through leveraging conceptor matrix representation [10], a computational model inspired by neuroscience, to more flexibly manage overlapping tasks' vector subspaces in continual learning. Conceptor matrices model the task subspaces based on input feature vectors, encoding the importance of directions in the input space of previous tasks and enabling selective updating for new tasks. By encoding past knowledge in conceptor matrices, CODE-CL enables a more comprehensive yet controlled exploration of the weight space, allowing learning to occur in previously restricted areas that do not interfere with critical directions from past tasks.

A core contribution of CODE-CL lies in its adaptive mechanism for task overlap analysis. We introduce a method to analyze overlap by computing intersection subspaces among tasks based on their conceptor representations, identifying highly correlated tasks with substantial shared feature space. For these correlated tasks, CODE-CL employs a gradient projection strategy that allows the model to learn a scaled projection within the intersection subspace. This approach promotes efficient forward knowledge transfer, leveraging shared information between tasks to enhance performance on new tasks without significant interference with previously learned knowledge. For less correlated tasks, CODE-CL constrains updates to avoid disrupting prior knowledge, preserving task-specific information effectively. Furthermore, we conduct extensive evaluations on widely used continual learning benchmarks in image classification, such as Permuted MNIST [15], Split CIFAR100 [13], Split miniImageNet [29], and 5-Datasets [5], to demonstrate the efficacy of CODE-CL. The results show that CODE-CL consistently achieves superior performance with minimal forgetting across tasks, outperforming several comparable state-of-the-art continual learning methods. In summary, CODE-CL provides a scalable, memory-efficient approach that enables both retention of past knowledge and the flexible acquisition of new information. The main contributions of this work are summarized as:

- Introduce a novel continual learning method, CODE-CL, that leverage the conceptors' pseudo-Boolean algebra for promoting retention of past knowledge and flexible acquisition of new information.
- Validate effectiveness of the proposed method extensively on multiple continual image classification benchmarks achieving performance superior to most of the state-of-the-art gradient projection methods.

2. Background

In this section, we outline essential properties of conceptor matrices that are central to our approach and provide an overview of related work in continual learning.

2.1. Conceptor matrices

Conceptor matrices are a computational model inspired by neuroscience [10]. This mathematical framework was introduced to encode and control the dynamics of recurrent neural networks [10]. Given a batch of feature vectors $\boldsymbol{X} \in \mathbb{R}^{b \times n}$, where b is the batch size and n is the dimension of the feature vector space, a conceptor matrix $\boldsymbol{C}(\boldsymbol{X}, \alpha)$ is defined as the solution to the following minimization problem:

$$\boldsymbol{C}(\boldsymbol{X}, \alpha) = \arg\min_{\boldsymbol{C}} \frac{1}{b}\|\boldsymbol{X} - \boldsymbol{X}\boldsymbol{C}\|_F^2 + \alpha^{-2}\|\boldsymbol{C}\|_F^2 \quad (1)$$

Here, $\alpha \in (0, \infty)$ is called the aperture and serves as a regularization factor. Also, note that this optimization problem has a closed-form solution:

$$\boldsymbol{C}(\boldsymbol{X}, \alpha) = \frac{\boldsymbol{X}^\top \boldsymbol{X}}{b}\left(\frac{\boldsymbol{X}^\top \boldsymbol{X}}{b} + \alpha^{-2}\boldsymbol{I}\right)^{-1} \quad (2)$$

Therefore, given the singular value decomposition (SVD) of the matrix $\boldsymbol{X} = \boldsymbol{U}\boldsymbol{\Sigma}\boldsymbol{V}^\top$, the conceptor matrix can be expressed as $\boldsymbol{C} = \boldsymbol{U}\boldsymbol{S}\boldsymbol{U}^\top = \boldsymbol{U}\boldsymbol{\Sigma}^2(\boldsymbol{\Sigma}^2 + b\alpha^{-2}\boldsymbol{I})^{-1}\boldsymbol{U}^\top$. Thus, the singular values of $\boldsymbol{C}$ lie between 0 and 1 ($0 < S_{i,i} < 1, \forall i \in \{0, 1, \ldots, n\}$), representing the importance of a particular direction $\boldsymbol{U}_{:,i}$ in the feature vector space $\boldsymbol{X}$. In this way, $\boldsymbol{C}$ acts as a soft projection matrix onto the linear subspace of the feature vectors of $\boldsymbol{X}$.

One important feature of the conceptor matrices is that those satisfy most laws of Boolean logic, as described by Jaeger [10], allowing to define a pseudo-Boolean algebra that provide a simple and intuitive framework to handle the linear subspaces defined within a conceptor matrix. Some of the boolean operations supported by conceptor matrices are NOT ($\neg$), OR ($\vee$), and AND ($\wedge$). Specifically, for two conceptor matrices ($\boldsymbol{C}$ and $\boldsymbol{B}$), the operations are defined as follows:

$$\neg\boldsymbol{C} = \boldsymbol{I} - \boldsymbol{C} \quad (3)$$

$$\boldsymbol{C} \wedge \boldsymbol{B} = (\boldsymbol{C}^{-1} + \boldsymbol{B}^{-1} - \boldsymbol{I})^{-1} \quad (4)$$

$$\boldsymbol{C} \vee \boldsymbol{B} = \neg(\neg\boldsymbol{C} \wedge \neg\boldsymbol{B}) \quad (5)$$

Here $\neg\boldsymbol{C}$ can be interpreted as a soft projection onto a linear subspace that is the pseudo-orthogonal complement of the subspace characterized by $\boldsymbol{C}$. Moreover, $\boldsymbol{C} \wedge \boldsymbol{B}$ compute the conceptor matrix that describes approximately a space that lies in the intersection between the subspaces characterized by $\boldsymbol{C}$ and $\boldsymbol{B}$. Similarly, $\boldsymbol{C} \vee \boldsymbol{B}$ describes approximately the union between the linear subspaces represented by $\boldsymbol{C}$ and $\boldsymbol{B}$.
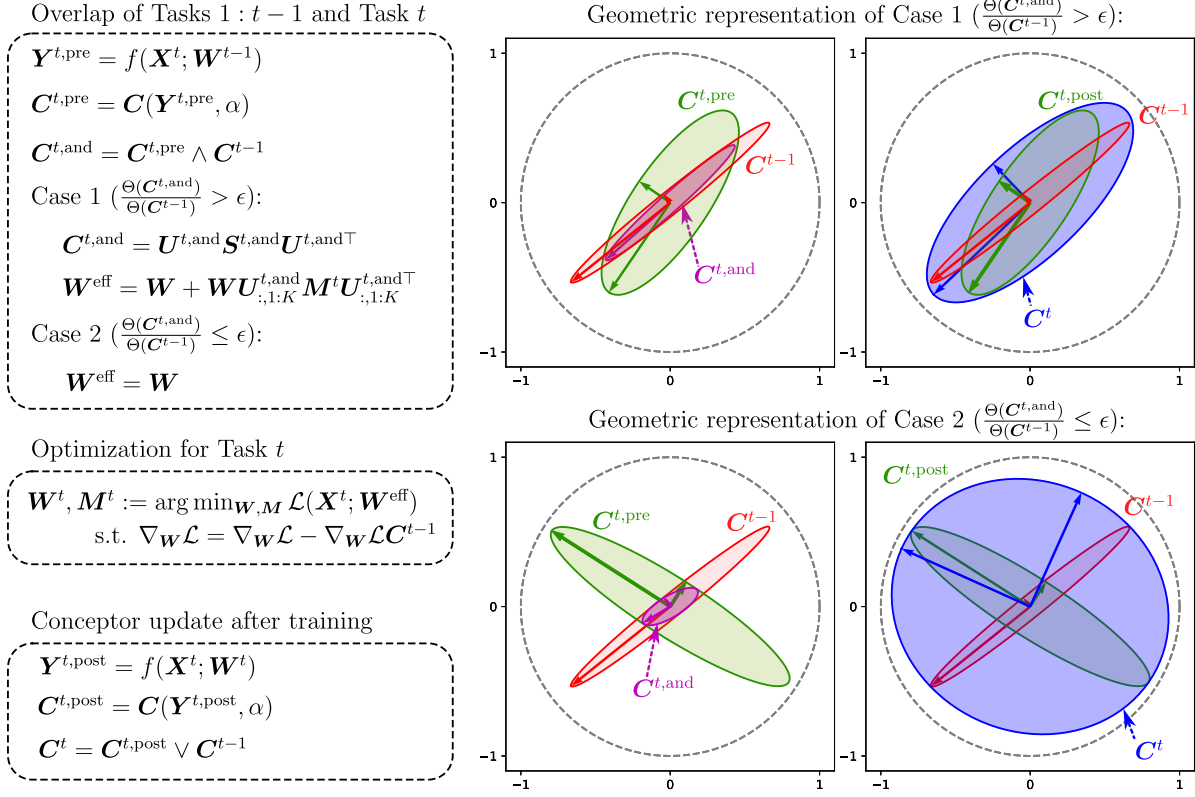
Figure 1. CODE-CL procedure for learning Task t after learning sequentially Task 1 to Task $t-1$. The first step involves analyzing the intersection between the conceptors $\boldsymbol{C}^{t-1}$ and $\boldsymbol{C}^{t,\text{pre}}$, which represent the input space for tasks 1 to $t-1$, and the current task t before training, respectively. Such intersection space is represented by the conceptor $\boldsymbol{C}^{t,\text{and}} = \boldsymbol{C}^{t-1} \wedge \boldsymbol{C}^{t,\text{pre}}$. So, if $\boldsymbol{C}^{t,\text{and}}$ capacity ($\Theta(\boldsymbol{C}^{t,\text{and}})$) is greater than certain threshold (ϵ) of the $\Theta(\boldsymbol{C}^{t-1})$, then it means that there is a high correlation between the current tasks and all the previous tasks, so to achieve high performance on the current task, we allow the model to learn on the top K dimensions of the intersection subspace ($\boldsymbol{C}^{t,\text{and}}$) by projecting the weights into that subspace using square matrix $\boldsymbol{M} \in \mathbb{R}^{K \times K}$. In this manner, the effective weights ($\boldsymbol{W}^{\text{eff}}$) become a projection of the actual weights and projected weights, and allows learning without affecting the previous tasks. Otherwise, if $\Theta(\boldsymbol{C}^{t,\text{and}})/\Theta(\boldsymbol{C}^{t-1})$ ratio is lower than ϵ, then there is low correlation between task therefore the complementary subspace of $\boldsymbol{C}^{t-1}$ ($\neg \boldsymbol{C}^{t-1}$), must be enough to learn the current task successfully, so the effective weight remains unchanged ($\boldsymbol{W}^{\text{eff}} = \boldsymbol{W}$). Afterward, optimization proceeds as usual, subject to the gradients of the weights ($\nabla_{\boldsymbol{W}} \mathcal{L}$) projected onto the complementary subspace ($\neg \boldsymbol{C}^{t-1}$) of the previous tasks. Once training is complete, we consolidate the knowledge of the current task by computing a new conceptor matrix, $\boldsymbol{C}^{t,\text{post}}$, and merging it with $\boldsymbol{C}^{t-1}$. In this manner a new conceptor representing all the tasks from 1 to t is obtained as $\boldsymbol{C}^t = \boldsymbol{C}^{t,\text{post}} \vee \boldsymbol{C}^{t-1}$.

The aperture parameter α plays a crucial role in determining how information is stored in the conceptors, as it scales the energy of the feature vectors ($\boldsymbol{X}_{:,i}$) stored in them. Aperture adaptation for a conceptor $\boldsymbol{C}(\boldsymbol{X}, \alpha)$ is defined by:

$$\psi(\boldsymbol{C}, \beta) = \boldsymbol{C}(\boldsymbol{C} + \beta^{-2}(\boldsymbol{I} - \boldsymbol{C}))^{-1} = \boldsymbol{C}(\boldsymbol{X}, \alpha\beta) \quad (6)$$

Here, the function $\psi(\boldsymbol{C}, \beta)$ scales the aperture factor of the conceptor $\boldsymbol{C}$ by a factor of β.

Also, we can measure the capacity, or memory usage, of a conceptor matrix based on the mean value of their singular values $S_{i,i}$ as:

$$\Theta(\boldsymbol{C}) = \frac{1}{n} \sum_{i=0}^{n} S_{i,i} \quad (7)$$

A capacity of 0 would indicate that the conceptor is empty and can be represented as a null matrix, while a capacity of 1 would indicate that the conceptor memory is full, becoming in practice, an identity matrix.

In summary, conceptors provide a powerful framework for handling concepts encoded in the linear subspaces where the feature vectors lie, which we leverage for continual learning in deep neural networks. This section offers only a brief overview of the key properties of conceptors relevant to our work.

2.2. Related works

Continual learning (CL) is a challenging problem where models need to learn new tasks sequentially without for-

getting previously learned knowledge. Several methods have been proposed to address this, which can be broadly classified into expansion-based, regularization-based, and memory-based approaches [16, 25, 30].

2.2.1. Regularization-based methods

These methods aim to mitigate forgetting by penalizing changes to important model parameters. Elastic Weight Consolidation (EWC) [12] utilizes the Fisher information matrix to estimate the importance of each parameter, applying this as a regularization term in the loss function to preserve essential parameters across tasks. Similar strategies are employed in [22, 26]. Other methods, such as the approach in [36], measure parameter importance based on each parameter's contribution to overall loss variation. In contrast, methods like Hard Attention to Task (HAT) [27] and PackNet [18] utilize attention masks or binary weight masks to control the update of neurons relevant to previous tasks. Although these methods are effective at protecting essential parameters, they often rely on complex heuristics to determine parameter importance or require storing multiple model versions, which significantly increases memory.

2.2.2. Expansion-based methods

These techniques tackle catastrophic forgetting by increasing the model's capacity as new tasks are introduced. Progressive Neural Networks (PNNs) [23] freeze the parameters of the previous tasks while expanding the network with new sub-networks for each task. Methods like RCL [32] and BNS [20] expand the network model based on a reinforcement learning strategy. Dynamically Expandable Networks (DEN) [33] combine strategies like model compression and network expansion to optimize task-specific architectures. While effective in isolating tasks to prevent interference, these approaches often lead to significant network growth, which makes them resource-intensive.

2.2.3. Memory-based methods

These approaches mitigate catastrophic forgetting by retaining information, either as stored samples or gradient-related information, from previous tasks. Experience Replay (ER) [2, 21] retains a subset of past task data to be replayed alongside new tasks, effectively reinforcing knowledge retention. Gradient Episodic Memory (GEM) [17] and Averaged GEM (A-GEM) [3] employ stored gradient information to constrain updates in a way that prevents interference with previous tasks. Another category within memory-based methods is gradient-projection based approaches, which address forgetting without the need to store raw data from past tasks. These methods achieve this by projecting gradients orthogonally to prior task directions. For example, Orthogonal Weight Modulation (OWM) [35] learns a projection matrix that transforms gradients for new tasks minimizing interference. Similarly,

Conceptor-Aided Backpropagation (CAB) [9] utilizes conceptor matrices and regularization terms to project gradients into pseudo-orthogonal directions, preserving knowledge from earlier tasks. An alternative approach is presented in Gradient Projection Memory (GPM) [25], which applies singular value decomposition (SVD) to identify and store the most significant singular vectors. This process defines a subspace for each previous task, allowing subsequent gradients to be projected orthogonally to these task-specific subspaces. More recent methods such as TRGP [16] and SGP [24] build upon GPM to improve performance while maintaining low levels of forgetting. Specifically, TRGP defines "trusted region" projection subspaces within the subspace of previous tasks, enabling selective model updates by assessing the gradient projection magnitude for each prior task subspace as defined by GPM. In contrast, SGP relaxes the strict orthogonality requirement of GPM, allowing gradients to contain components that align partially with previous task subspaces. This modification provides a balance between effective knowledge transfer and retention.

3. CODE-CL: Conceptor-based Deep Continual Learning

In this section, we describe the steps of our COnceptor-based gradient projection for DEep Continual Learning (CODE-CL) method. We consider a supervised continual learning setting where T tasks are learned sequentially, with each task having sufficient labeled samples. We explore both domain-incremental and task-incremental learning scenarios in this supervised setting [30].

Each task is identified by $t \in \mathbb{T} = \{1, 2, \ldots, T\}$, and its associated dataset is represented as $\mathbb{D}^t = \{(\boldsymbol{x}_i^t, y_i^t)_{i=1}^{n_t}\}$, where n_t is the number of samples, $\boldsymbol{x}_i^t$ is the input sample, and y_i^t is the corresponding label. Using these datasets, we train a neural network with parameters $\mathbb{W}^t = \{(\boldsymbol{W}^{(l),t})_{l=1}^{L}\}$, where L is the model's number of layers.

For all tasks beyond the first, learning follows a three-step process: (1) Analyzing the overlap of the input space between the current task and previous tasks, using their respective conceptor matrices, (2) training the model on the current task with gradients constrained to subspaces defined by previous tasks' conceptor matrices, and (3) merging the information of the current and previous tasks into an updated conceptor matrix. As each layer follows the same procedure, the following discussion focus on a single layer.

3.1. Learning on Task $t = 1$

For the initial task, learning proceeds with random weight initialization, $\boldsymbol{W} = \boldsymbol{W}^0$, and the model is trained on dataset $\mathbb{D}^1$ by minimizing a loss function:

$$\boldsymbol{W}^1 := \arg\min_{\boldsymbol{W}} \mathcal{L}(\boldsymbol{W}; \mathbb{D}^1) \tag{8}$$

Optimization is performed using minibatch stochastic gradient descent (SGD) without constraints. After training concludes based on set criteria, we compute a conceptor matrix $\boldsymbol{C}^1$ to encode the input subspace layer-wise. Specifically, we randomly sample a batch of inputs from $\mathbb{D}^1$, forming $\boldsymbol{X}^1 = [\boldsymbol{x}_1^{1\top}, \boldsymbol{x}_2^{1\top}, \dots, \boldsymbol{x}_b^{1\top}]$, where b denotes batch size. Based on (2), we compute the conceptor $\boldsymbol{C}^1 = \boldsymbol{C}(\boldsymbol{X}^1, \alpha)$ with aperture α. This process is repeated for each layer by forward propagating inputs through the model, so each layer has its own conceptor matrix. As discussed in Section 2, the singular values $S_{i,i}$ of the conceptor represent the importance of each direction, guiding which directions are preserved for new tasks.

3.2. Learning on Task $t \in \{2, 3, \dots, T\}$

For each new task, we follow a three-step process, as illustrated in Fig. 1.

3.2.1. Task overlap analysis: Tasks $1 : t - 1$ and Task t

Before training on task t, we analyze the overlap between its input space and that of previous tasks, represented by $\boldsymbol{C}^{t-1}$. In order to do this, we compute a conceptor matrix for task t. First, we sample a batch of samples from $\mathbb{D}^t$ to construct $\boldsymbol{X}^{(0),t,\mathrm{pre}}$, where the superscript 'pre' indicates pre-training status. Then, for hidden layers, we propagate inputs forward through the model with weights from the prior task, $\boldsymbol{W}^{t-1}$, to obtain $\boldsymbol{X}^{(l),t,\mathrm{pre}} = f(\boldsymbol{X}^{(l-1),t,\mathrm{pre}}; \boldsymbol{W}^{(l),t-1})$, where $f(\cdot)$ denotes the model's non-linear function (e.g ReLU). We then compute the pre-training conceptor for task t as $\boldsymbol{C}^{t,\mathrm{pre}} = \boldsymbol{C}(\boldsymbol{X}^{t,\mathrm{pre}}, \alpha)$. The input space overlap is represented by the intersection $\boldsymbol{C}^{t,\mathrm{and}} = \boldsymbol{C}^{t,\mathrm{pre}} \wedge \boldsymbol{C}^{t-1}$, depicted geometrically in Fig. 1. The similarity between $\boldsymbol{C}^{t,\mathrm{and}}$ and $\boldsymbol{C}^{t-1}$ indicates task correlation. So, if many directions for the current task are encoded in $\boldsymbol{C}^{t-1}$, tasks are highly correlated. Task correlation is measured by the capacity ratio between conceptor matrices (7), defining high (low) correlation when the ratio surpasses (falls below) a threshold ϵ:

Case 1 ($\frac{\Theta(\boldsymbol{C}^{t,\mathrm{and}})}{\Theta(\boldsymbol{C}^{t-1})} > \epsilon$): In this high-correlation scenario (illustrated in Fig. 1), directions encoded in $\boldsymbol{C}^{t-1}$ are important for task t. The model is permitted to learn in the top K directions of $\boldsymbol{C}^{t,\mathrm{and}}$ without disturbing prior tasks. To achieve this, weights are projected onto the subspace defined by the top K directions and optimized using a matrix $\boldsymbol{M} \in \mathbb{R}^{K \times K}$:

$$\boldsymbol{W}^{t,\mathrm{eff}} = \boldsymbol{W} + \boldsymbol{W}\boldsymbol{U}_{:,1:K}^{t,\mathrm{and}} \boldsymbol{M}^t \boldsymbol{U}_{:,1:K}^{t,\mathrm{and}\top} \quad (9)$$

Here, $\boldsymbol{U}_{:,1:K}^{t,\mathrm{and}}$ are the top-K singular vectors of $\boldsymbol{C}^{t,\mathrm{and}}$. This is explicitly allowing to effectively forward transfer knowledge form old tasks to the current task.

Case 2 ($\frac{\Theta(\boldsymbol{C}^{t,\mathrm{and}})}{\Theta(\boldsymbol{C}^{t-1})} \le \epsilon$): In this low-correlation case, task overlap is minimal, so no previous directions need adjusting. Thus, the effective weights remain as $\boldsymbol{W}^{t,\mathrm{eff}} = \boldsymbol{W}$.

3.2.2. Optimization for task t

With $\boldsymbol{W}^{t,\mathrm{eff}}$ defined, weights are initialized as $\boldsymbol{W} = \boldsymbol{W}^{t-1}$, and the model is trained on $\mathbb{D}^t$ to minimize a loss function:

$$\begin{aligned} \boldsymbol{W}^t, \boldsymbol{M}^t &:= \arg\min_{\boldsymbol{W},\boldsymbol{M}} \mathcal{L}(\boldsymbol{W}^{t,\mathrm{eff}}; \mathbb{D}^t) \\ &\mathrm{s.t.} \nabla_{\boldsymbol{W}}\mathcal{L} = \nabla_{\boldsymbol{W}}\mathcal{L}(\boldsymbol{I} - \boldsymbol{C}^{t-1}) \end{aligned} \quad (10)$$

Minibatch SGD optimizes the weights with gradients constrained to lie in the pseudo-orthogonal subspace of the conceptor matrix defined by $\neg\boldsymbol{C}^{t-1}$. This process continues until certain stopping criteria are met.

3.2.3. Conceptor update after training on task t

After training, we merge current and past task knowledge into a new conceptor matrix. Firsr, a new post-training conceptor matrix $\boldsymbol{C}^{t,\mathrm{post}}$ is computed by sampling a batch from $\mathbb{D}^t$, constructing $\boldsymbol{X}^{(0),t,\mathrm{post}}$, and forward propagating through the model using the updated weights $\boldsymbol{W}^t$, similarly to Section 3.2.1. The layer-wise conceptor matrix for task t post-training is $\boldsymbol{C}^{t,\mathrm{post}} = \boldsymbol{C}(\boldsymbol{X}^{t,\mathrm{post}}, \alpha)$. We then merge $\boldsymbol{C}^{t,\mathrm{post}}$ and $\boldsymbol{C}^{t-1}$ into a new conceptor matrix consolidating all learned tasks: $\boldsymbol{C}^t = \boldsymbol{C}^{t,\mathrm{post}} \vee \boldsymbol{C}^{t-1}$, illustrated in Fig. 1.

4. Experimental evaluation

In this section, we present an empirical assessment of CODE-CL, demonstrating its effectiveness across multiple continual learning image classification benchmarks. Our evaluation focuses on measuring the method's ability to retain prior knowledge while adapting to new tasks, comparing its performance against other CL approaches.

4.1. Experimental Setup

This subsection describes the general experimental setup applied across all evaluations of CODE-CL. We outline the benchmarks and models, training details, and metrics, to ensure consistent and fair evaluation.

4.1.1. Benchmarks and models:

We evaluate our method on widely used continual learning (CL) benchmarks, including Permuted MNIST [15], Split CIFAR100 [13], Split miniImageNet [29], and 5-Datasets [5]. The Permuted MNIST benchmark is a variation of the MNIST dataset where the pixel positions of each image are randomly permuted, creating distinct versions of the original images for each class. In our experiments, we use ten sequential tasks, each with a different permutation, and train a three-layer fully connected network with 100 neurons in each hidden layer, similar to the setup in [16, 17, 25], in a

Table 1. Performance comparison on continual image classification datasets using multi-head networks. Accuracy and BWT (mean ± std) are reported over five trials. Best results are in bold and second best are underlined. [†],[‡] and [*] denote the results from [25], [16] and [24] respectively

Method	Split CIFAR100		Split MiniImageNet		5-Datasets	
	ACC (%)	BWT (%)	ACC (%)	BWT (%)	ACC (%)	BWT (%)
Multitask[†]	79.58 ± 0.54	–	69.46 ± 0.62	–	91.54 ± 0.28	–
OWM [35][†]	50.94 ± 0.60	-30 ± 1	–	–	–	–
EWC [12][†]	68.80 ± 0.88	-2 ± 1	52.01 ± 2.53	-12 ± 3	88.64 ± 0.26	-4 ± 1
HAT [27][†]	72.06 ± 0.50	0 ± 0	59.78 ± 0.57	-3 ± 0	91.32 ± 0.18	-1 ± 0
A-GEM [3][†]	63.98 ± 1.22	-15 ± 2	57.24 ± 0.72	-12 ± 1	84.04 ± 0.33	-12 ± 1
ER_Res [2][†]	71.73 ± 0.63	-6 ± 1	58.94 ± 0.85	-7 ± 1	80.31 ± 0.22	-4 ± 0
GPM [25][†]	72.48 ± 0.40	-0.9 ± 0	60.41 ± 0.61	-0.7 ± 0.4	91.22 ± 0.20	-1 ± 0
TRGP [16][‡]	74.46 ± 0.32	-0.9 ± 0.01	61.78 ± 0.60	-0.5 ± 0.6	$\mathbf{93.56 \pm 0.10}$	-0.04 ± 0.01
SGP [24][*]	$\underline{76.05 \pm 0.43}$	-1.0 ± 0	$\underline{62.83 \pm 0.33}$	-1.5 ± 1	–	–
CODE-CL (Ours)	$\mathbf{77.21 \pm 0.32}$	-1.1 ± 0.28	$\mathbf{68.83 \pm 0.41}$	-1.1 ± 0.3	$\underline{93.32 \pm 0.13}$	-0.25 ± 0.02

domain-incremental setting. For Split CIFAR100, the original CIFAR100 dataset is divided into T groups, each containing an equal number of classes $(100/T)$. In our experiments, we split the dataset into 10 groups, with each group representing a separate task, and train a 5-layer AlexNet model in a multi-head setting, where each task has its own output head, following the methodology of [16, 24, 25]. Similarly, the Split miniImageNet benchmark consists of a subset of 100 classes from the ImageNet dataset, divided into T groups. For our experiments, we split the dataset into 20 groups, each containing 5 classes, and trained a reduced ResNet18 architecture in a multi-head setting, as done in prior works [16, 24, 25]. The 5-Datasets benchmark involves training a model sequentially on five different datasets, CIFAR10, MNIST, SVHN, notMNIST, and Fashion MNIST, with each dataset treated as a single task. For this benchmark, we again use a reduced ResNet18 model in a multi-head setting. In all experiments, we refrained from using data augmentation to align with prior works. The dataloaders for Split CIFAR100 and 5-Datasets were sourced from [25], while those for Permuted MNIST and Split mini-ImageNet were provided by the Avalanche library [1].

4.1.2. Training details:

For all our experiments we use vanilla stochastic gradient descent (SGD), with dynamic learning rate reduction based on a validation metric and using early stopping criteria. Each task in Split CIFAR100 is trained for 200 epochs with a batch size of 64 with an aperture $\alpha = 6$, similarly, each task on Split miniImageNet and 5-Datasets is trained for a maximum of 100 epochs with a batch size of 64, with $\alpha = 8$ and $\alpha = 4$ respectivetly. Additionally, each task on Permuted MNIST is trained for 5 epochs with a batch size of 100 with $\alpha = 3$. All the experiments reported on Table 1 and Table 2 used $K = 80$. More details of training

setup, hyperparameters and implementation are given in the Supplementary Material.

4.1.3. Metrics:

Similar to previous works [16, 17, 25], we use two metrics to evaluate the performance of our method, such as: the average final accuracy over all tasks, Accuracy (ACC), and Backward Transfer (BWT), which measures the forgetting of old tasks when learning new tasks. ACC and BWT are defined as:

$$\text{ACC} = \sum_{i=1}^{T} \frac{A_{T,i}}{T} \; ; \text{BWT} = \sum_{i=1}^{T-1} \frac{A_{T,i} - A_{i,i}}{T-1} \qquad (11)$$

Here, T is the number of tasks, $A_{j,i}$ is the accuracy of the model on i-th task after learning the j-th task sequentially $(i \le j)$.

4.2. Results

In this subsection, we present the performance of CODE-CL in comparison with prior approaches, along with a detailed analysis of its memory complexity. Additionally, we conduct ablation studies to assess the impact of varying the number of free dimensions, K, on the method's performance.

4.2.1. Performance Comparison:

As shown in Table 1 and Table 2, our method demonstrates high accuracy with minimal forgetting across all benchmarks. Specifically, CODE-CL consistently delivers competitive results, outperforming previous methods on most datasets.

On Permuted MNIST, Table 2, CODE-CL surpasses existing methods such as GPM and TRGP in terms of accuracy. Moreover, on Split CIFAR100, CODE-CL achieves an impressive accuracy of 77.21%, coming close to the

Table 2. Performance comparison on the Permuted MNIST dataset using a single network in a domain incremental setting. Accuracy and BWT (mean ± std) are reported over five trials. Best results are in bold and second best are underlined. † and ‡ denote the results from [25] and [16] respectively

Method	Permuted MNIST	
	ACC (%)	BWT (%)
Multitask†	96.70 ± 0.02	–
OGD [6]†	82.56 ± 0.66	-14 ± 1
OWM [35]†	90.71 ± 0.11	-1 ± 0
EWC [12]†	89.97 ± 0.57	-4 ± 1
A-GEM [3]†	83.56 ± 0.16	-14 ± 1
ER_Res [2]†	87.24 ± 0.53	-11 ± 1
GPM [25]†	93.91 ± 0.16	-3 ± 0
TRGP [16]‡	$\underline{96.34 \pm 0.11}$	-0.8 ± 0.1
CODE-CL (Ours)	$\mathbf{96.56 \pm 0.06}$	-0.24 ± 0.04

upper bound set by Multitask learning (79.58%), which serves as an ideal, but unrealistic, comparison point. Notably, CODE-CL outperforms other state-of-the-art continual learning methods, registering 4.73%, 2.75%, and 1.16% higher accuracy than GPM, TRGP, and SGP, respectively. Similarly, on Split MiniImageNet, CODE-CL once again performs exceptionally well, achieving an accuracy second only to Multitask learning, and outperforming GPM by 8.42%, TRGP by 7.05%, and SGP by 6%. This further underscores CODE-CL's robustness, particularly when handling more challenging datasets, where competing methods tend to experience significant performance drops. On the 5-Datasets benchmark, CODE-CL reaches an accuracy of 93.32%, outperforming GPM by 2.1% and Multitask learning by 1.78%. Although it falls just 0.24% short of TRGP on this benchmark, the difference is marginal, highlighting CODE-CL's strong overall performance across diverse tasks.

In terms of backward transfer (BWT), our results further illustrate the effectiveness of CODE-CL in mitigating catastrophic forgetting. On Permuted MNIST, CODE-CL achieves a BWT of -0.24%, which is lower than previous methods like GPM and TRGP. Furthermore, on Split CIFAR100, CODE-CL records a BWT of -1.1%, indicating minimal performance loss on previously learned tasks, and this result is comparable to those obtained by GPM, TRGP, and SGP. Likewise, on Split MiniImageNet, CODE-CL reports a BWT of -1.1%, which is consistent with state-of-the-art methods, demonstrating its capacity to retain learned knowledge with minimal degradation. Finally, in the 5-Datasets benchmark, CODE-CL achieves a BWT of -0.25%, outperforming GPM and performing slightly worse than TRGP. In summary, the high accuracy and low forgetting of CODE-CL highlight its ability to effec-

(a) Split CIFAR100 (ACC) (b) Split CIFAR100 (BWT)

(c) Split miniImageNet (ACC) (d) Split miniImageNet (BWT)

(e) 5-Datasets (ACC) (f) 5-Datasets (BWT)

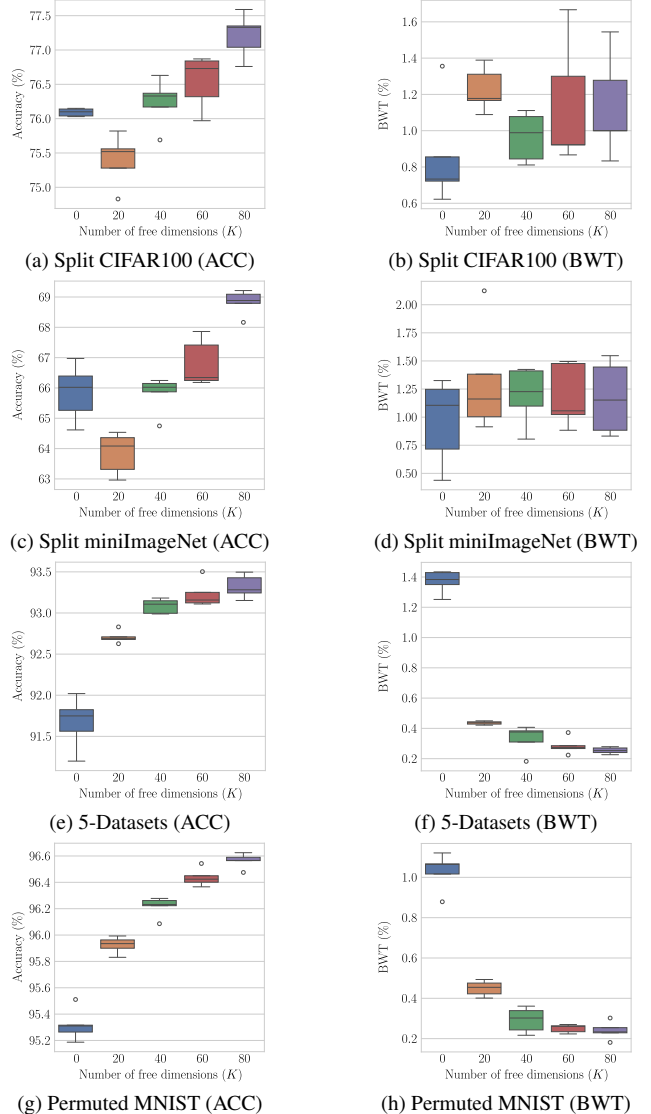(g) Permuted MNIST (ACC) (h) Permuted MNIST (BWT)

Figure 2. Effect of the number of free dimensions (K) parameter on the final accuracy and BWT for the Split CIFAR100, Split mini-ImageNet, 5-Datasets, and Permuted MNIST benchmarks. The box plots were generated based on the results of five independent runs.

tively balance the trade-off between plasticity and stability, maintaining strong performance across a range of continual learning tasks while minimizing forgetting.

4.2.2. Memory Complexity:

Efficient memory usage is crucial, especially when scaling to larger networks and a greater number of tasks. In this section, we compare the memory complexity of our proposed method against other established methods, including GPM, TRGP, and SGP.

For simplicity, the following analysis focuses on a sin-

Table 3. Memory complexity comparison among methods. The analysis is done for a single fully-connected layer with N inputs, M outputs, after being trained on T tasks. Also, B is the average number of important direction per task used in [16] and K is the number of free dimensions parameter used in CODE-CL.

Methods	GPM	TRGP	SGP	CODE-CL (Ours)
Memory Complexity	$O(N^2)$	$O(N^2 + TNB + TB^2)$	$O(N^2)$	$O(N^2 + TNK + TK^2)$

gle fully-connected layer with N inputs and M outputs after training sequentially on T tasks. For CODE-CL, the memory complexity is influenced by the conceptor matrices that has a dimension N^2 that encode the information of the input vector space, more over as discussed in Section 3, CODE-CL uses a discrete fixed number of free dimensions per task (K) to learn the an optimal linear combination of the K most important direction of the subspace represented by the intersection of the conceptor of old tasks with the new task. This term incurs into additional memory proportional to $TKN + TK^2$, where TKN represent the K most important direction of dimension N for T tasks. Therefore, reaching a memory complexity of $O(N^2 + TNK + TK^2)$ In the case of GPM and SGP, the additional memory usage is determine by the dimension of the inputs N, the number of important directions per task B and the number of tasks T. So the maximum dimension in those cases is in the order of $O(N^2)$. Finally, TRGP requires the same memory than GPM to store the important direction of all learned tasks, but in addition to this, TRGP requires to store the important directions per tasks as well as the important direction in the trusted region projection subspaces, which incur in additional memory $TNB + TB^2$. Table 3 summarizes the memory complexity for each method.

Note that, as the methods scale for deeper models, the number of free dimension used in our method is fixed and significantly less than the dimension of the input space, $K \ll N$, which make the ratio between memories requirements of GPM and CODE-CL close to ~ 1. However, for deeper models B scales with the size of the model, therefore the memory of TRGP becomes dominated by the term TNB, which make the method essentially require $\sim B/K$ times more memory than our method.

4.2.3. Effect of K in performance:

To investigate the influence of the number of free dimensions (K) on model performance, we conduct ablation studies using different values of K. The results for all four benchmarks are presented in Fig. 2. In general, we observe that increasing K enhances model accuracy while maintaining a low Backward Transfer (BWT). However, this trend varies across the benchmarks, revealing two distinct patterns.

For the 5-Datasets and Permuted MNIST benchmarks, increasing K consistently improves accuracy and substantially reduces BWT. In contrast, for Split CIFAR100 and

Split miniImageNet, the model achieves higher accuracy when $K \geq 40$, while setting $K = 20$ leads to a small accuracy decline. Moreover, in these latter benchmarks, higher values of K slightly increase BWT, though the effect remains relatively minor. These contrasting results can be attributed to the nature of the benchmarks. In the 5-Datasets and Permuted MNIST benchmarks, the tasks are inherently diverse, as the images originate from distinct distributions with minimal overlap. Conversely, the tasks in Split CIFAR100 and miniImageNet are derived from a shared distribution, leading to greater overlap among tasks. Consequently, while increasing K generally enhances accuracy by facilitating knowledge transfer from previous tasks to new tasks, the reduction in BWT is less pronounced for tasks with significant data distribution overlap. The similarity in data distributions across tasks in Split CIFAR100 and miniImageNet likely limits BWT reduction, even as accuracy benefits from a larger K.

5. Conclusions

The ability to learn incrementally, retaining past knowledge while adapting to new information, is essential for continual learning in artificial neural networks. This work proposed CODE-CL, a novel continual learning method that leverages conceptor-based gradient projection. CODE-CL addresses the limitations of traditional gradient projection by employing conceptor matrices, a model inspired by neuroscience, allowing the model to flexibly manage overlapping task's subspaces for continual learning. By encoding past tasks into conceptor matrices, CODE-CL enables a nuanced approach to managing shared and unique information across tasks, facilitating both knowledge retention and efficient forward transfer. The method's adaptive mechanism analyzes task overlap, enhancing the model's ability to leverage shared knowledge between tasks without compromising performance on previously learned tasks. Extensive evaluations on diverse continual learning benchmarks, including Split CIFAR100, Split miniImageNet, 5-Datasets, and Permuted MNIST, demonstrate CODE-CL's superior performance and reduced forgetting compared to other comparable state-of-the-art methods. CODE-CL's ability to dynamically allocate memory for correlated and independent tasks makes it scalable and efficient for real-world applications where adaptability to evolving environments is essential.

Acknowledgments

References

[1] Antonio Carta, Lorenzo Pellegrini, Andrea Cossu, Hamed Hemati, and Vincenzo Lomonaco. Avalanche: A PyTorch Library for Deep Continual Learning. *Journal of Machine Learning Research*, 24(363):1–6, 2023. 6

[2] Arslan Chaudhry, Marcus Rohrbach Facebook, A I Research, Mohamed Elhoseiny, Thalaiyasingam Ajanthan, Puneet K Dokania, Philip H S Torr, and Marc ' Aurelio Ranzato. On Tiny Episodic Memories in Continual Learning. *arXiv:1902.10486*, 2019. 1, 4, 6, 7

[3] Arslan Chaudhry, Marc'Aurelio Ranzato, Marcus Rohrbach, and Mohamed Elhoseiny. Efficient Lifelong Learning with A-GEM. *International Conference on Learning Representations*, 2019. 1, 4, 6, 7

[4] Danruo DENG, Guangyong Chen, Jianye Hao, Qiong Wang, and Pheng-Ann Heng. Flattening Sharpness for Dynamic Gradient Projection Memory Benefits Continual Learning. *Advances in Neural Information Processing Systems*, 34: 18710–18721, 2021. 2

[5] Sayna Ebrahimi, Franziska Meier, Roberto Calandra, Trevor Darrell, and Marcus Rohrbach. Adversarial Continual Learning. In *Computer Vision – ECCV 2020: 16th European Conference, Glasgow, UK, August 23–28, 2020, Proceedings, Part XI*, pages 386–402, Berlin, Heidelberg, 2020. Springer-Verlag. 2, 5

[6] Mehrdad Farajtabar, Navid Azizan, Alex Mott, Ang Li, Deepmind Caltech, and Deepmind Deepmind. Orthogonal Gradient Descent for Continual Learning. In *Proceedings of the Twenty Third International Conference on Artificial Intelligence and Statistics*, pages 3762–3773. PMLR, 2020. 1, 7

[7] Yiduo Guo, Wenpeng Hu, Dongyan Zhao, and Bing Liu. Adaptive Orthogonal Projection for Batch and Online Continual Learning. *Proceedings of the AAAI Conference on Artificial Intelligence*, 36(6):6783–6791, 2022. 1

[8] Raia Hadsell, Dushyant Rao, Andrei A. Rusu, and Razvan Pascanu. Embracing Change: Continual Learning in Deep Neural Networks. *Trends in Cognitive Sciences*, 24(12): 1028–1040, 2020. 1

[9] Xu He and H. Jaeger. Overcoming Catastrophic Interference using Conceptor-Aided Backpropagation. *International Conference on Learning Representations*, 2018. 1, 4

[10] Herbert Jaeger. Controlling Recurrent Neural Networks by Conceptors. *arXiv:1403.3369*, 2014. 2, 1

[11] E. R. Kandel and R. D. Hawkins. The biological basis of learning and individuality. *Scientific American*, 267(3):79–86, 1992. 1

[12] James Kirkpatrick, Razvan Pascanu, Neil Rabinowitz, Joel Veness, Guillaume Desjardins, Andrei A. Rusu, Kieran Milan, John Quan, Tiago Ramalho, Agnieszka Grabska-Barwinska, Demis Hassabis, Claudia Clopath, Dharshan Kumaran, and Raia Hadsell. Overcoming catastrophic forgetting in neural networks. *Proceedings of the National Academy of Sciences of the United States of America*, 114 (13):3521–3526, 2017. 1, 4, 6, 7

[13] Alex Krizhevsky. Learning Multiple Layers of Features from Tiny Images. 2009. 2, 5

[14] Dhireesha Kudithipudi, Mario Aguilar-Simon, Jonathan Babb, Maxim Bazhenov, Douglas Blackiston, Josh Bongard, Andrew P. Brna, Suraj Chakravarthi Raja, Nick Cheney, Jeff Clune, Anurag Daram, Stefano Fusi, Peter Helfer, Leslie Kay, Nicholas Ketz, Zsolt Kira, Soheil Kolouri, Jeffrey L. Krichmar, Sam Kriegman, Michael Levin, Sandeep Madireddy, Santosh Manicka, Ali Marjaninejad, Bruce McNaughton, Risto Miikkulainen, Zaneta Navratilova, Tej Pandit, Alice Parker, Praveen K. Pilly, Sebastian Risi, Terrence J. Sejnowski, Andrea Soltoggio, Nicholas Soures, Andreas S. Tolias, Darío Urbina-Meléndez, Francisco J. Valero-Cuevas, Gido M. van de Ven, Joshua T. Vogelstein, Felix Wang, Ron Weiss, Angel Yanguas-Gil, Xinyun Zou, and Hava Siegelmann. Biological underpinnings for lifelong learning machines. *Nature Machine Intelligence 2022 4:3*, 4(3):196–210, 2022. 1

[15] Yann LeCun, Corinna Cortes, and C J Burges. MNIST handwritten digit database. *ATT Labs [Online]. Available: http://yann.lecun.com/exdb/mnist*, 2, 2010. 2, 5

[16] Sen Lin, Li Yang, Deliang Fan, and Junshan Zhang. TRGP: Trust Region Gradient Projection for Continual Learning. *International Conference on Learning Representations*, 2022. 1, 2, 4, 5, 6, 7, 8

[17] David Lopez-Paz and Marc ' Aurelio Ranzato. Gradient Episodic Memory for Continual Learning. In *Proceedings of the 31st International Conference on Neural Information Processing Systems*, 2017. 1, 4, 5, 6

[18] Arun Mallya and Svetlana Lazebnik. PackNet: Adding Multiple Tasks to a Single Network by Iterative Pruning. *2018 IEEE/CVF Conference on Computer Vision and Pattern Recognition*, pages 7765–7773, 2017. 1, 4

[19] German I. Parisi, Ronald Kemker, Jose L. Part, Christopher Kanan, and Stefan Wermter. Continual lifelong learning with neural networks: A review. *Neural Networks*, 113:54–71, 2019. 1

[20] Qi Qin, Wenpeng Hu, Han Peng, Dongyan Zhao, and Bing Liu. BNS: Building Network Structures Dynamically for Continual Learning. *Advances in Neural Information Processing Systems*, 34:20608–20620, 2021. 1, 4

[21] Sylvestre Alvise Rebuffi, Alexander Kolesnikov, Georg Sperl, and Christoph H. Lampert. iCaRL: Incremental Classifier and Representation Learning. *2017 IEEE Conference on Computer Vision and Pattern Recognition (CVPR)*, 2017-January:5533–5542, 2017. 1, 4

[22] H. Ritter, Aleksandar Botev, and D. Barber. Online Structured Laplace Approximations For Overcoming Catastrophic Forgetting. *Neural Information Processing Systems*, 2018. 4

[23] Andrei A. Rusu, Neil C. Rabinowitz, Guillaume Desjardins, Hubert Soyer, James Kirkpatrick, Koray Kavukcuoglu, Raz-

van Pascanu, and Raia Hadsell. Progressive Neural Networks. *arXiv preprint arXiv:1606.04671*, 2016. 1, 4

[24] Gobinda Saha and Kaushik Roy. Continual Learning with Scaled Gradient Projection. *Proceedings of the 37th AAAI Conference on Artificial Intelligence, AAAI 2023*, 37:9677–9685, 2023. 1, 2, 4, 6

[25] Gobinda Saha, Isha Garg, and K. Roy. Gradient Projection Memory for Continual Learning. *International Conference on Learning Representations*, 2021. 1, 4, 5, 6, 7

[26] Jonathan Schwarz, Wojciech M. Czarnecki, Jelena Luketina, A. Grabska-Barwinska, Y. Teh, Razvan Pascanu, and R. Hadsell. Progress & Compress: A scalable framework for continual learning. *International Conference on Machine Learning*, 2018. 4

[27] J. Serrà, Dídac Surís, M. Miron, and Alexandros Karatzoglou. Overcoming catastrophic forgetting with hard attention to the task. *International Conference on Machine Learning*, 2018. 1, 4, 6

[28] Yujun Shi, Li Yuan, Yunpeng Chen, and Jiashi Feng. Continual Learning via Bit-Level Information Preserving. *2021 IEEE/CVF Conference on Computer Vision and Pattern Recognition (CVPR)*, pages 16669–16678, 2021. 1

[29] O. Vinyals, C. Blundell, T. Lillicrap, K. Kavukcuoglu, and Daan Wierstra. Matching Networks for One Shot Learning. *Neural Information Processing Systems*, 2016. 2, 5

[30] Liyuan Wang, Xingxing Zhang, Hang Su, and Jun Zhu. A Comprehensive Survey of Continual Learning: Theory, Method and Application. *IEEE Transactions on Pattern Analysis and Machine Intelligence*, 46(08):5362–5383, 2024. 1, 4

[31] Shipeng Wang, Xiaorong Li, Jian Sun, and Zongben Xu. Training Networks in Null Space of Feature Covariance for Continual Learning. *2021 IEEE/CVF Conference on Computer Vision and Pattern Recognition (CVPR)*, pages 184–193, 2021. 1

[32] Ju Xu and Zhanxing Zhu. Reinforced Continual Learning. In *Proceedings of the 32nd International Conference on Neural Information Processing Systems*, pages 907–916, 2018. 1, 4

[33] Jaehong Yoon, Eunho Yang, Jeongtae Lee, and Sung Ju Hwang. Lifelong Learning with Dynamically Expandable Networks. *International Conference on Learning Representations*, 2018. 4

[34] Jaehong Yoon, Saehoon Kim, Eunho Yang, and Sung Ju Hwang. Scalable and Order-robust Continual Learning with Additive Parameter Decomposition. *International Conference on Learning Representations*, 2020. 1

[35] Guanxiong Zeng, Yang Chen, Bo Cui, and Shan Yu. Continual learning of context-dependent processing in neural networks. *Nature Machine Intelligence 2019 1:8*, 1(8):364–372, 2019. 1, 4, 6, 7

[36] Friedemann Zenke, Ben Poole, and Surya Ganguli. Continual Learning Through Synaptic Intelligence. *Proceedings of machine learning research*, 70:3987, 2017. 1, 4

CODE-CL: <u>CO</u>nceptor-Based Gradient Projection for <u>DE</u>ep <u>C</u>ontinual <u>L</u>earning

Supplementary Material

A. Conceptor Implementation Details

We implement the conceptor operations following the equations presented in Section 2, with one exception: the AND operation (4).

As noted in [10], the operation defined in (4) is only valid when the conceptor matrices are invertible. However, in practice, since we use a limited number of samples to compute the conceptors, the resulting matrices are often not full rank. To address this, we adopt a more general version of the AND operation, as proposed in [10]:

$$C \wedge B = D(D^\top(C^\dagger + B^\dagger - I)D)^{-1}D^\top, \quad (12)$$

Here, $C^\dagger$ and $B^\dagger$ denote the pseudo-inverses of C and B, respectively. The matrix D consists of columns that form an arbitrary orthonormal basis for the intersection of the column spaces of C and B.

The procedure for computing D is outlined in Algorithm 1.

Algorithm 1 Computation of matrix D in (12)

Input: C, B, β (threshold), N (dimension of C and B)
Output: D
  $U_C, S_C \leftarrow \text{SVD}(C)$ ▷ Singular value decomposition
  $U_B, S_B \leftarrow \text{SVD}(B)$
  $k_C \leftarrow \text{num\_elements}(S_C > \beta)$ ▷ # of elements $> \beta$
  $k_B \leftarrow \text{num\_elements}(S_B > \beta)$
  $U'_C \leftarrow U_C[:, k_C :]$ ▷ Last $N - k_C$ columns
  $U'_B \leftarrow U_B[:, k_B :]$
  $U, S \leftarrow \text{SVD}(U'_C U'^\top_C + U'_B U'^\top_B)$
  $k \leftarrow \text{num\_elements}(S > \beta)$
  $D \leftarrow U[:, k :]$

B. Experimental Setup

This section provides details on the architecture of all models used in this work, the dataset statistics, the hyperparameters for each experiment, and the compute resources employed.

B.1. Model Architecture

In this work, we utilize two models: an AlexNet-like architecture, as described in [27], and a Reduced ResNet18 [17].

The AlexNet-like model incorporates batch normalization (BN) in every layer except the classifier layer. The BN layers are trained during the first task and remain frozen for subsequent tasks. The model consists of three convolutional layers with 64, 128, and 256 filters, using kernel sizes of 4×4, 3×3, and 2×2, respectively. These are followed by two fully connected layers, each containing 2048 neurons. ReLU activation functions are used throughout, along with 2×2 max-pooling layers after each convolutional layer. Dropout is applied with rates of 0.2 for the first two layers and 0.5 for the remaining layers.

The Reduced ResNet18 follows the architecture detailed in [25]. For the Split miniImageNet experiments, the first layer uses a stride of 2, while for the 5-Datasets benchmark, it uses a stride of 1.

For all models and experiments, cross-entropy loss is employed as the loss function.

B.2. Dataset Statistics

The statistics for the four benchmarks used in this work for continual image classification are summarized in Table 4 and Table 5. For all benchmarks, we follow the same data partitions as those used in [16, 24, 25].

For the 5-Datasets benchmark, grayscale images are replicated across all RGB channels to ensure compatibility with the architecture. Additionally, all images are resized to 32×32 pixels, resulting in an input size of $3 \times 32 \times 32$ for this benchmark.

B.3. Hyperparameters

The hyperparameters used in our experiments are detailed in Table 6.

B.4. Compute resources

All experiments were conducted on a shared internal Linux server equipped with an AMD EPYC 7502 32-Core Processor, 504 GB of RAM, and four NVIDIA A40 GPUs, each with 48 GB of GDDR6 memory. Additionally, code was implemented using Python 3.9 and PyTorch 2.2.1 with CUDA 11.8.

C. CODE-CL algorithm

The pseudo-code for CODE-CL is shown in Algorithm 2.

Algorithm 2 CODE-CL pseudo code

Input: $\mathbb{D}^t = \{(\boldsymbol{x}_i^t, y_i^t)_{i=1}^{n_t}\}$, $\mathbb{W} = \{(\boldsymbol{W}^{(l)})_{l=1}^L\}$, α (aperture), ϵ (threshold), η_0 (learning rate), E (number of epochs), b (batch size), η_{th} (minimum learning rate), b_s (batch size for computer computation), K (number of free dimensions)

$\mathbb{W} \leftarrow \mathbb{W}^0$ $\triangleright$ Random initialization

$epoch \leftarrow 0$

$\eta \leftarrow \eta_0$

while $epoch < E$ and $\eta > \eta_{th}$ **do** $\triangleright$ Learning on the first task ($t = 1$)

     for $n = 1, 2, \ldots, \lfloor \frac{n_1}{b} \rfloor$ **do**

         $\mathbb{B}_b \sim \mathbb{D}_{\text{train}}^1$ $\triangleright$ Sample of a mini-batch of size b from the train set of task 1 ($\mathbb{D}_{\text{train}}^1$)

         $\nabla_{\mathbb{W}}\mathcal{L} \leftarrow$ compute_gradient$(\mathbb{W}, \mathbb{B}_b)$

         $\mathbb{W} \leftarrow \mathbb{W} - \eta \nabla_{\mathbb{W}}\mathcal{L}$

     end for

     $epoch \leftarrow epoch + 1$

     $\eta \leftarrow$ LR_decay$(\mathbb{W}, \mathbb{D}_{\text{test}}^1, \eta)$

end while

$\mathbb{B}_{b_s} \sim \mathbb{D}_{\text{train}}^1$

$\mathbb{X}^1 \leftarrow$ forward$(\mathbb{W}, \mathbb{B}_{b_s})$ $\triangleright$ Set of inputs for all layers $\mathbb{X}^1 = \{(\boldsymbol{X}^{(l),1})_{l=1}^L\}$

$\mathbb{C}^1 \leftarrow$ compute_conceptor$(\mathbb{X}^1, \alpha)$ $\triangleright$ Compute conceptor matrices per layer ($\mathbb{C}^1 = \{(\boldsymbol{C}^{(l),1})_{l=1}^L\}$) based on (2)

$\mathbb{W}^{1,\text{eff}} \leftarrow \mathbb{W}^1$

for $t = 2, 3, \ldots, T$ **do** $\triangleright$ Learning on Task $t \in \{2, 3, \ldots, T\}$

     $\mathbb{B}_{b_s} \sim \mathbb{D}_{\text{train}}^t$

     $\mathbb{X}^t \leftarrow$ forward$(\mathbb{W}^{t-1,\text{eff}}, \mathbb{B}_{b_s})$

     $\mathbb{C}^{t,\text{pre}} \leftarrow$ compute_conceptor$(\mathbb{X}^t, \alpha)$

     $\mathbb{C}^{t,\text{and}} \leftarrow \mathbb{C}^{t,\text{pre}} \wedge \mathbb{C}^{t-1}$ $\triangleright$ AND operation based on (4)

     for $l = 1, 2, \ldots, L$ **do**

         if $\frac{\Theta(\boldsymbol{C}^{(l),t,\text{and}})}{\Theta(\boldsymbol{C}^{(l),t-1})} > \epsilon$ **then**

            $\boldsymbol{U}^{(l),t} \leftarrow$ SVD$(\boldsymbol{C}^{(l),t,\text{and}})$ $\triangleright$ Singular value decomposition

            $\boldsymbol{M}^{(l),t} \sim \mathcal{N}$ $\triangleright$ Random initialization of matrix $\boldsymbol{M} \in \mathbb{R}^{K \times K}$

            $\boldsymbol{W}^{(l),t,\text{eff}} \leftarrow \boldsymbol{W}^{(l)}(\boldsymbol{I} - \boldsymbol{U}_{:,1:K}^{(l),t} \boldsymbol{M}^{(l),t} \boldsymbol{U}_{:,1:K}^{(l),t\top})$

         else

            $\boldsymbol{W}^{(l),t,\text{eff}} \leftarrow \boldsymbol{W}^{(l)}$

         end if

     end for

     $\mathbb{W}^{t,\text{eff}} \leftarrow \{(\boldsymbol{W}^{(l),t,\text{eff}})_{l=1}^L\}$

     $epoch \leftarrow 0$

     $\eta \leftarrow \eta_0$

     while $epoch < E$ and $\eta > \eta_{th}$ **do**

         for $n = 1, 2, \ldots, \lfloor \frac{n_1}{b} \rfloor$ **do**

            $\mathbb{B}_b \sim \mathbb{D}_{\text{train}}^t$

            $\nabla_{\mathbb{W}}\mathcal{L}, \nabla_{\mathbb{M}^t}\mathcal{L} \leftarrow$ SGD$(\mathbb{W}^{t,\text{eff}}, \mathbb{B}_b)$

            $\nabla_{\mathbb{W}}\mathcal{L} \leftarrow \nabla_{\mathbb{W}}\mathcal{L} - \nabla_{\mathbb{W}}\mathcal{L}\mathbb{C}^{t-1}$ $\triangleright$ Gradient projection per layer $\nabla_{\boldsymbol{W}^{(l)}}\mathcal{L} \leftarrow \nabla_{\boldsymbol{W}^{(l)}}\mathcal{L} - \nabla_{\boldsymbol{W}^{(l)}}\mathcal{L}\boldsymbol{C}^{(l),t-1}$

            $\mathbb{W} \leftarrow \mathbb{W} - \eta \nabla_{\mathbb{W}}\mathcal{L}$

            $\mathbb{M}^t \leftarrow \mathbb{M}^t - \eta \nabla_{\mathbb{M}^t}\mathcal{L}$

         end for

         $epoch \leftarrow epoch + 1$

         $\eta \leftarrow$ LR_decay$(\mathbb{W}, \mathbb{D}_{\text{test}}^t, \eta)$

     end while

     $\mathbb{B}_{b_s} \sim \mathbb{D}_{\text{train}}^t$

     $\mathbb{X}^t \leftarrow$ forward$(\mathbb{W}, \mathbb{B}_{b_s})$ $\triangleright$ Set of inputs for all layers $\mathbb{X}^t = \{(\boldsymbol{X}^{(l),t})_{l=1}^L\}$

     $\mathbb{C}^{t,\text{post}} \leftarrow$ compute_conceptor$(\mathbb{X}^t, \alpha)$

     $\mathbb{C}^t \leftarrow \mathbb{C}^{t,\text{post}} \vee \mathbb{C}^{t-1}$ $\triangleright$ Compute conceptor matrices for Task t based on (5)

end for

Table 4. Permuted MNIST, Split CIFAR100 and Split miniImageNet datasets statistics.

Dataset	Permuted MNIST	Split CIFAR100	Split miniImageNet
Number of tasks (T)	10	10	20
Sample dimensions	$1 \times 28 \times 28$	$3 \times 32 \times 32$	$3 \times 84 \times 84$
Number of classes per task	10	10	5
Training samples per task	54000	4750	2375
Validation samples per task	6000	250	125
Test samples per task	10000	1000	500

Table 5. 5-Datasets statistics.

Dataset	CIFAR10	MNIST	SVHN	Fashion MNIST	notMNIST
Number of classes	10	10	10	10	10
Training samples	47500	57000	69595	57000	16011
Validation samples	2500	3000	3662	3000	842
Test samples	10000	10000	26032	10000	1873

Table 6. List of hyperparameters used in our experiments.

Dataset	Permuted MNIST	Split CIFAR100	Split miniImageNet	5-Datasets
Learning rate (η)	0.01	0.01	0.1	0.1
Batch size (b)	100	64	64	64
Batch size for conceptor comp. (b_s)	300	125	125	125
Min. learning rate (η_{th})	—	10^{-5}	10^{-5}	10^{-3}
Learning rate decay factor	—	1/2	1/2	1/3
Patience	—	6	6	5
Number of epochs (E)	5	200	100	100
Aperture (α)	3	6	8	4
Threshold (ϵ)	0.5	0.5	0.5	0.5